micromachines

MDPI

Article

Dynamical Control of Broadband Coherent Absorption in ENZ Films

Vincenzo Bruno [1], Stefano Vezzoli [2], Clayton DeVault [3,4], Thomas Roger [5], Marcello Ferrera [5], Alexandra Boltasseva [3,4], Vladimir M. Shalaev [3,4] and Daniele Faccio [1,*]

1 School of Physics and Astronomy, University of Glasgow, Glasgow G12 8QQ, UK; v.bruno.1@research.gla.ac.uk
2 The Blackett Laboratory, Department of Physics, Imperial College London, London SW7 2BW, UK; s.vezzoli@imperial.ac.uk
3 Purdue Quantum Science and Engineering Institute, Purdue University, 1205 West State Street, West Lafayette, IN 47907, USA; devaultx@gmail.com (C.D.); aeb@purdue.edu (A.B.); shalaev@purdue.edu (V.M.S.)
4 School of Electrical and Computer Engineering and Birck Nanotechnology Center, Purdue University, 1205 West State Street, West Lafayette, IN 47907, USA
5 Institute of Photonics and Quantum Sciences, Heriot-Watt University, Edinburgh EH14 4AS, UK; thomas.roger@gmail.com (T.R.); M.Ferrera@hw.ac.uk (M.F.)
* Correspondence: daniele.faccio@glasgow.ac.uk

Received: 12 December 2019; Accepted: 16 January 2020; Published: 20 January 2020

Abstract: Interferometric effects between two counter-propagating beams incident on an optical system can lead to a coherent modulation of the absorption of the total electromagnetic radiation with 100% efficiency even in deeply subwavelength structures. Coherent perfect absorption (CPA) rises from a resonant solution of the scattering matrix and often requires engineered optical properties. For instance, thin film CPA benefits from complex nanostructures with suitable resonance, albeit at a loss of operational bandwidth. In this work, we theoretically and experimentally demonstrate a broadband CPA based on light-with-light modulation in epsilon-near-zero (ENZ) subwavelength films. We show that unpatterned ENZ films with different thicknesses exhibit broadband CPA with a near-unity maximum value located at the ENZ wavelength. By using Kerr optical nonlinearities, we dynamically tune the visibility and peak wavelength of the total energy modulation. Our results based on homogeneous thick ENZ media open a route towards on-chip devices that require efficient light absorption and dynamical tunability.

Keywords: transparent conductive oxide; coherent perfect absorption; epsilon-near-zero media; light-with-light modulation; refractive index change

1. Introduction

Coherent perfect absorption (CPA) was first proposed as a time-reversed version of a laser [1]. Similar to a laser cavity, CPA occurs when light is resonant at specific wavelengths in a high-Q Fabry–Perot optical resonator. However, for CPA, the active gain material is replaced with a moderately lossy medium. Because the system's single-pass losses are typically low, perfect absorption for a given input intensity is extremely sensitive to the Q-factor and resonance wavelength [2,3].

An alternative scheme utilizes deeply subwavelength and highly absorbing materials [4–6]. Here, two counter-propagating coherent beams interfere at the film's surface and create a standing wave. Absorption in the film is then modulated by changing the relative phase of the two beams, or equivalently by scanning the film along the nodes (peak transmittance) and antinodes (peak absorption) of the interference pattern. This approach has been demonstrated in the ultrafast [7]

and quantum regime [8–11], as well as in integrated photonic systems [12–16]. While a resonant cavity is not required, single-pass absorption should be 50% to achieve perfect absorption [17,18]. This is difficult to obtain in conventional dielectrics (too little losses) or metals (too high reflectivity). To circumnavigate this challenge, metasurfaces—nanostructured subwavelength films—with ideal absorptive optical properties have been used to achieve CPA [4,19]. Ideal absorption can be achieved in extremely subwavelength films over a broad range of wavelengths, making metasurface-based CPA advantageous over bulk cavity structures and compatible with integrated photonic platforms [3].

While metasurfaces and other engineered structures can exhibit CPA over large wavelength ranges, the necessary nanofabrication can be a limitation for practical CPA applications. Thin films of epsilon-near-zero (ENZ) materials, such as transparent conductive oxides (TCOs) like aluminum-doped zinc oxide (AZO) or indium tin oxide (ITO), have been proposed as a particularly suitable platform for broadband CPA [20]. ENZ materials exhibit a real part of the dielectric permittivity which crosses zero for wavelengths of practical interest in the near-infrared or visible regions [21,22]. Due to the continuity of the transverse component of the electric field at the interface, the electric field within the ENZ material can be very large and can lead to perfect absorption (PA) when illuminated at a critical angle of incidence [23,24]. In the limit of deeply subwavelength ENZ film, PA is provided by critical coupling the incident light to a fast wave propagating along the ENZ layer [24]. The proposed systems for ENZ PA are multilayer structures where the ENZ thin layer is sandwiched between two dielectrics or a dielectric and a metal structure [25]. At the critical angle where CPA happens (this is often referred to as directional PA), the loss follows a linear relationship with the ENZ film thickness which implies that CPA can occur in an arbitrarily thin ENZ film (with arbitrary small single-pass absorption) [26]. For instance, PA has been demonstrated for films of ITO film thickness as low as 0.02 λ_0 (free-space wavelength) and with only 5% single-pass absorption [27]. Electrical tuning of one port directional PA have also been shown in plasmonic strip cavity based on a ENZ thin layer, with a modulation in reflectance of the 15% [28]. Finally, broadband coherent modulation of directional PA in ENZ deeply subwavelength film have been proved by using ITO multylayer structures sandwiched between two ZnSe prisms [20]. The control of nonlinear processes by two port illumination was also theorized for deeply sub-wavelength ENZ slab [29]. Applications of CPA in deeply subwavelength ENZ films could be found in photovoltaic energy conversion or devices such as bolometers which require large absorption with small masses. However, other applications, such as in nonlinear or quantum optics, may benefit from thicker films where the efficiency of the nonlinear process and the parametric gain generally scale with thickness.

Here, we study CPA in films of TCOs near their ENZ wavelength where the film's refractive index exhibits large anomalous dispersion and a near-zero refractive index. Such films can be treated as deeply subwavelength because the effective wavelength will increase drastically for wavelength approaching the ENZ wavelength. We theoretically and experimentally explore the role of this transition region in order to achieve CPA in homogeneous AZO optically thick films and then show how this can be controlled with intense optical pump fields. It was recently shown that the combination of low refractive index and the high damage threshold of these materials allows TCOs to exhibit large and ultrafast Kerr-type optical nonlinearities in the ENZ region [30–36] and behave as efficient time-varying medium [37,38].

We perform CPA experiments in a Sagnac-like interferometer where two counter propagating light pulses are incident normal to the sample. We achieve coherent control of absorption in AZO films with different thicknesses. For all samples the total energy modulation exhibits a maximum value near the ENZ wavelength. We then demonstrate dynamical control of CPA using its strong intensity-dependent refractive index change. Our demonstration of broadband and tunable CPA in homogeneous ENZ films is relevant for practical nanoscale optical-switches and modulators where alternative nano-pattered metasurfaces would suffer from low switching efficiencies and detriments of nanofabrication processes.

2. Theoretical Investigation

Our optical system consists in two counter-propagating continuous waves (CW) impinging on a homogeneous ENZ film, E_{in}^{A} and E_{in}^{B}, respectively, at normal incidence (Figure 1a). From the transfer matrix method (TMM), we calculate the electric field at the two outputs of our symmetric system, E_{out}^{C} and E_{out}^{D} respectively. By changing the relative phase ϕ between the two counter-propagating beams, we simulate the scenario in which the film is shifted along the propagation direction and calculate the intensity of the two outputs, C and D (Figure 1b). By summing the intensity at the two outputs ($I_{Tot} = I_C + I_D$), we define the modulation visibility of the total energy as

$$V_{tot} = \frac{(I_{Tot}^{max} - I_{Tot}^{min})}{(I_{Tot}^{max} + I_{Tot}^{min})} \tag{1}$$

where I_{Tot}^{max} and I_{Tot}^{min} are the maximum and minimum of the total output energy of the system. In principle, for CPA to occur in a thin film, the transmission and reflection coefficients from both sides of the film should be equal ($|r| = |t|$) with a phase difference of $\varphi_{rt} = 0$ or π in order to achieve 100% light absorption. In this situation, the value of the total visibility is 1.

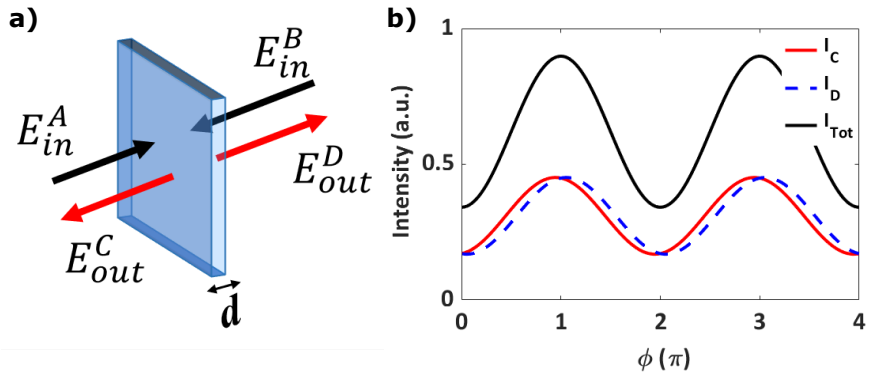

Figure 1. (**a**) Bi-directional coherent perfect absorption (CPA) scheme. (**b**) Intensity of the two output beams, C and D, and its sum as we scan the sample position in the propagation direction. This is equivalent to changing the relative phase between the two input fields ϕ.

We consider three different cases by fixing the zero crossing of the real part of the dielectric permittivity at $\lambda_{ENZ} \approx 1350$ nm, but vary the dispersion across the ENZ region as shown in Figure 2a–c where we plot the refractive index profiles (real, n, and imaginary, k, parts) for three different cases studied. These are calculated from a Drude model

$$\epsilon = \epsilon_\infty - \frac{\omega_p^2}{(\omega^2 + i\gamma\omega)} \tag{2}$$

where ϵ_∞ is the high frequency permittivity, ω_p is the plasma frequency and γ is the damping coefficient. It has been shown that this model correctly reproduces the ENZ refractive index for a variety of materials, as ITO and AZO [33,39–41]. In our case, we use $\epsilon_\infty = 3.18$ and $\omega_p = 2.4745 \times 10^{15}$ rad/s. We vary the Drude model damping coefficient, thus increasing losses and reducing the dispersion gradient in n, from (a) to (c) $\gamma = 1.0073 \times 10^{13} \rightarrow 2.4745 \times 10^{14}$ rad/s. Figure 2d–f show the visibility V_{tot} of the total energy as a function of the ENZ film's thickness for the three cases shown in Figure 2a–c. In Figure 2d (γ_a), we do not observe coherent modulation of the total energy for thickness below 1000 nm. Due to the high transmission of the thin film, the interference between the reflected and transmitted field is weak. For thicker films, r and t become more similar and stronger interference is observed. The TMM model predicts visibility with a maximum value close to one that is pinned to a wavelength slightly shorter than λ_{ENZ}. When we increase the optical losses of the ENZ slab, Figure 2e,f, the peak of the visibility becomes broader, exhibiting multiple resonances as the thickness

increases but all with maximum absorption at a wavelength just below λ_{ENZ}. These results show that the system exhibits broadband coherent modulation of the energy with a maximum value close to one just below λ_{ENZ}, independently of the thickness and of the single-pass absorption. We associate this maximum to a Fabry–Perot (FP) like resonance due to interference effects in the Air/AZO/glass system. The fact that the FP resonance is 'locked' before the ENZ wavelength irrespectively of the thickness is due to the ENZ condition [42,43].

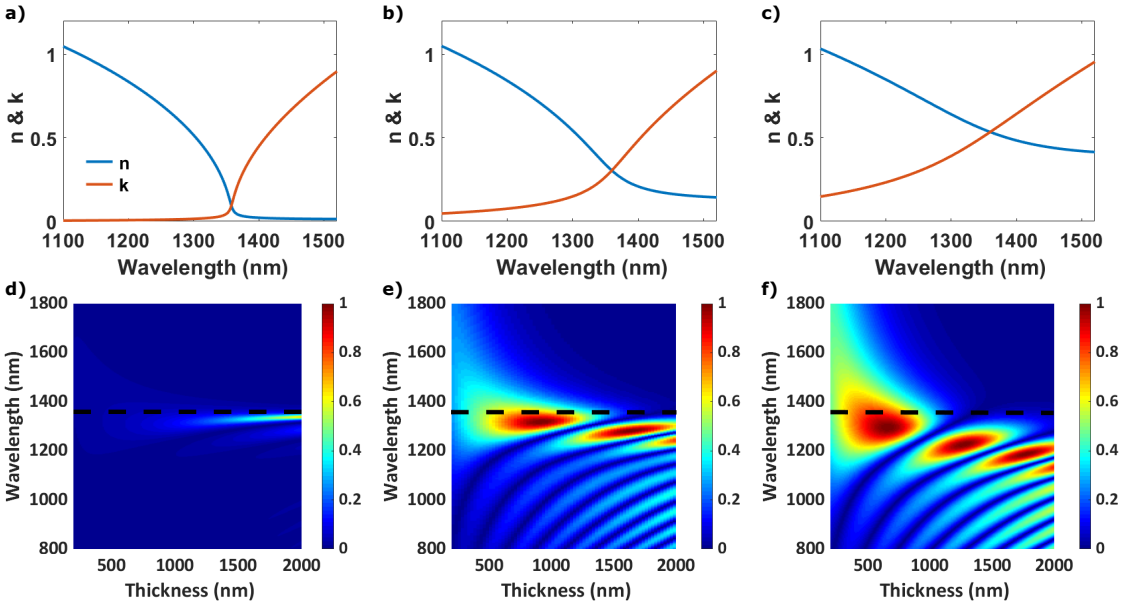

Figure 2. (**a**–**c**) Real and imaginary part of the refractive index of the three cases with $\lambda_{ENZ} \approx 1350$ nm. (**d**–**f**) Normalized visibility of the total energy as a function of the wavelength for different thicknesses. The dashed red line indicates the λ_{ENZ}. For the dispersion we use $\epsilon_\infty = 3.18$ and $\omega_p = 2.4745 \times 10^{15}$ rad/s. For the damping constant we use $\gamma_a = 1.0073 \times 10^{13}$, $\gamma_b = 0.8053 \times 10^{14}$ and $\gamma_c = 2.3614 \times 10^{14}$ rad/s.

In the ideal case without losses, the first resonance of an FP cavity is reached when the $2nd = \lambda_0$. Due to the strong gradient of the n before the ENZ region, the λ_0 at which the first resonance occurs will not scale linearly with d, but it will be locked in this spectral range with strong dispersion. Moreover, in a lossy dielectric medium, r and t become complex and their phases depend on the value of both n and k of the lossy medium. Here the first resonant order for the FP cavity is reached when $2nd = \lambda_0(1 - \alpha/\pi)$, where α is the phase of the transmission coefficient [18]. Combining the strong dispersion of n due to the ENZ condition and the value of k, almost perfect modulation of absorption is expected at wavelength just below λ_{ENZ} even for subwavelength thickness (Figure 2f).

3. Coherent Absorption and Its Dynamical Control

We experimentally investigated the behaviour of CPA in ENZ films using AZO films illuminated by two counter-propagating laser beams in a Sagnac-like interferometer configuration. Figure 3a shows a schematic of the set-up. Laser pulses (105 fs FWHM duration, repetition rate 100 Hz) are generated by an Optical Parametric Amplifier (TOPAS) in a tunable range between 1120 nm and 1500 nm. The input power is controlled through a half wave plate and a polarizing beam splitter, which also fixes the input p-polarization (horizontal in the lab frame). The beam is split by a non-polarizing beam splitter into two beams A and B with equal energy and then recombined onto the sample at normal incidence. The AZO film (deposited on a 1 mm thick glass slide) is facing the beam A, whereas the beam B is incident on the substrate side. The two beams are focused down to 50 µm by using a pair of 125 mm lenses. By moving the sample with a piezo-electric stage, interferograms are generated at the output C and D and measured with photodiodes. We used two beam splitters to extract the light from the

interferometer and send it to the photodiodes. A representative example of these interferograms are shown in Figure 3b. In order to calculate the energy visibility in the pulsed case we proceed in the same way as for the CW case, i.e. we evaluate the central portion (where the pulse intensity is maximum) of the interferogram and extrapolate the average values for maximum and minimum of the intensity.

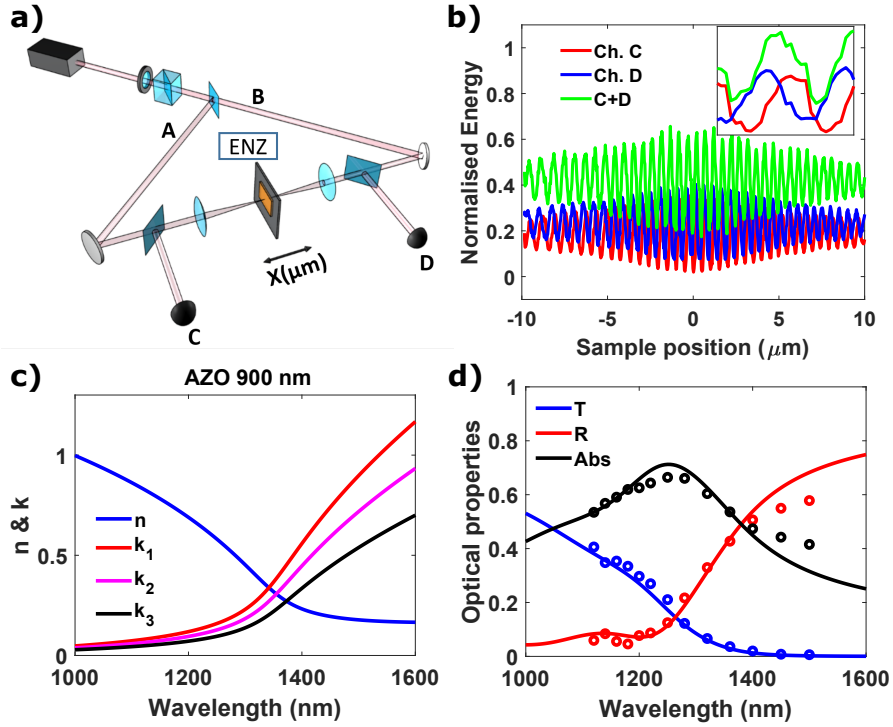

Figure 3. (**a**) Schematics of the Sagnac interferometer. (**b**) An example of measurement for λ_0 = 1280 nm, assuming energy equal to 1 at the interferometer input. The total modulation of the energy (or absorption) is given by the sum of C and D (green curve). The inset shows a zoom of the interferogram. (**c**) ellipsometer measurement of the index of refraction of AZO 900 nm thick film, (**d**) experimental (dots) and TMM simulation (solid line) of R, T and abs for the same sample.

We investigated two AZO samples of similar optical properties, i.e., n and k, in the ENZ region, but with thicknesses of 500 and 900 nm (Figure 3c). The real part of the dielectric permittivity crosses zero around 1340 nm for the 900-nm-thick film, which corresponds to where the real and imaginary part of the refractive index are equal ($n_{900} = k_{900} = 0.34$). For the 500-nm-thick sample the λ_{ENZ} is redshifted by 30 nm ($n_{500} = k_{500} = 0.52$ at the λ_{ENZ}) due to small differences in the material deposition. In the spectral range under analysis, n of the AZO 900-nm-thick film passes from close to 1 around 1100 nm to less than 0.2 for longer wavelengths. Since $\lambda_{eff} = \lambda_0/n$ inside the medium, the effective length ($L_{eff} = L/\lambda_{eff}$) of our sample is 0.8 λ_0 at 1050 nm, 0.21 λ_0 at the ($\lambda_{ENZ} = 1350$ nm, and becomes optically deeply subwavelength around 1500 nm (0.1 λ_0).

We also deposited three 900-nm-thick AZO films on a glass substrate three samples with similar n (about 20% difference), but different value of k at the crossing point ($k_1 = 0.34$, $k_2 = 0.30$ and $k_3 = 0.27$ for the 900 nm thick film). All the samples exhibit similar optical properties with an absorption close to 60% across the ENZ region (Figure 3d).

We first perform a CPA experiment for the bare glass substrate. In this case the energy modulation is almost zero for all the spectral range of interest. In Figure 4 we report the measured normalized total energy modulation visibility (red circles), together with the values predicted by the TMM (solid lines) for the AZO film. All the samples show the same trend independently from the thickness. In the case of high optical losses, for the different thicknesses the visibility is almost zero in the region where the index of refraction is close to one, whereas it increases and reaches a maximum value up to the 60% just before λ_{ENZ}. As we decrease the value of k, the trend of the visibility remains the same for all

the samples, but its maximum value across the transition region decreases. Overall, the experimental results confirm the predictions that CPA can be observed in ENZ films over a broad bandwidth with thicknesses larger than the conventional subwavelength designs. The bandwidth of ∼100 nm is comparable with CPA in deeply subwavelength ENZ single layer (∼150 nm [20]) or white-light cavity (∼100 nm [3]), whereas it is larger than metasurfaces (∼40 nm [4]).

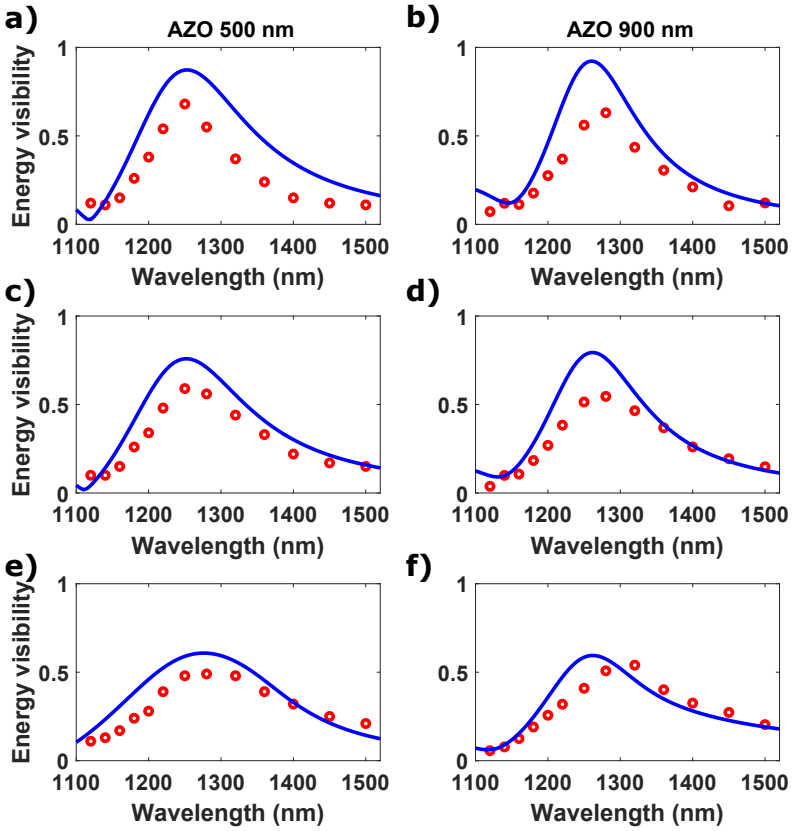

Figure 4. Experimental (circles) and transfer matrix method (TMM) simulation (solid line) of normalized visibility of the total energy for aluminum-doped zinc oxide (AZO) 500 nm and 900 nm with different values of k. (**a**,**b**) High losses k_1, (**c**,**d**) middle losses k_2 and (**e**,**f**) low losses k_3. For the TMM simulation we suppose $\Delta\lambda$ ∼60 nm.

We finally investigate nonlinear coherent absorption in ENZ films based on modification of the film refractive index through the nonlinear Kerr coefficient. Previously it has been demonstrated that the ENZ condition leads to the enhancement of third order nonlinearities in terms of nonlinear refractive index change for thin film of AZO [32]. This is based on the observation that when the permittivity is close to zero, any nonlinear change Δn, proportional to $\chi^{(3)}/n$, is enhanced due to the n tending to low values. In Ref. [32] a refractive index change of 400% was reported for an AZO film optically pumped with 1.3 TW/cm^2 without showing damage of the sample or saturation of the optical Kerr effect. In the same work, at λ = 1310 nm a nonlinear susceptibility of $Re[\chi^{(3)}] \sim 4.73 \times 10^{-20}$ V^2/m^2 and $Im[\chi^{(3)}] \sim 0.57 \times 10^{-20}$ V^2/m^2 was extrapolated. We therefore illuminated the AZO film in the Sagnac interferometer with two high intensity pulses at normal incidence and same wavelength. The intensities on each side are 0.8 and 0.6 TW/cm^2, respectively. By increasing the intensities from the linear regime to these maximum values, we observe that the CPA visibility passes from 68% of the linear case to 35% (Figure 5a,b). The peak of the normalized visibility also redshifts and becomes broader for both the samples, with a nearly 50 nm-shift for

the 500 nm sample. Following the recent works in TCOs, this can be explained by the fact that the dielectric permittivity, and so the optical constants including λ_{ENZ}, exhibit a redshift when it is optically pumped across the ENZ wavelength [31,44]. The redshift of the λ_{ENZ} is also associated to a positive Δn and to a negative Δk [30,32]. Due to the decreasing of k, the visibility drops, as we observed for the linear case. While, the shift of the visibility peak is related to the shift of λ_{ENZ} in the same direction, and therefore to the shift of the strong dispersion which the material exhibits at wavelength shorter than the zero-crossing frequency. In Figure 5c,d we plot the experimental results together with TMM simulations. The TMM simulations are obtained considering a ∼60 nm shift of ω_p and a decreasing of γ ($0.15 \times 10^{15} \rightarrow 0.09 \times 10^{15}$). This correspond to a $\Delta\lambda_{ENZ} \sim 60$ nm and to a $k_{500} = 0.38$ and $k_{900} = 0.24$. These results show that enhanced nonlinearities in ENZ materials can be used to add a degree of freedom to tune the efficiency and the bandwidth of coherent absorption.

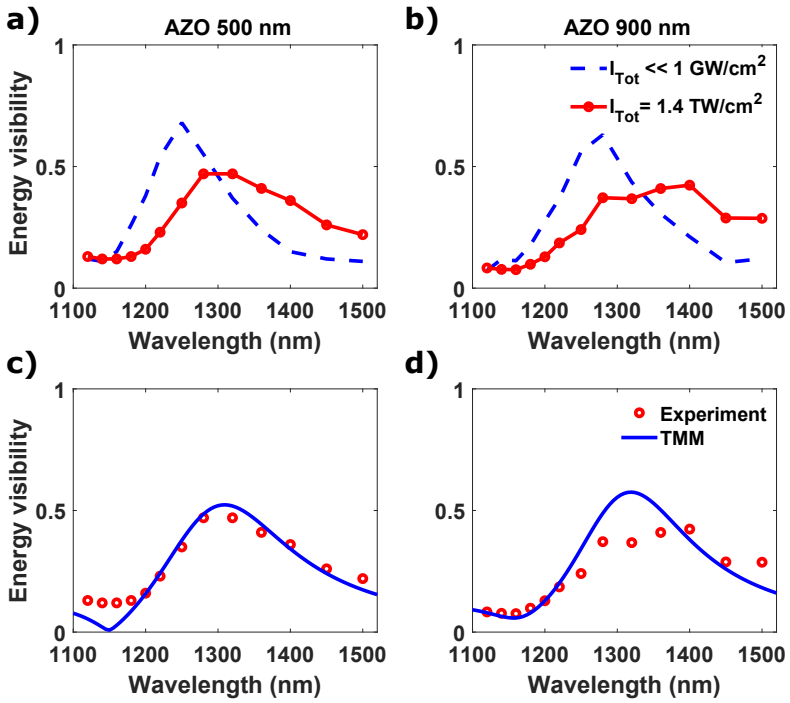

Figure 5. (**a**,**b**) Normalized visibility of the total energy for both samples, 500 nm (**a**) and 900 nm (**b**). The dashed blue curve represents the linear characterization, while the circles is the nonlinear CPA with high beam intensity. (**c**,**d**) Experimental (circles) and TMM simulation (solid line) of normalized visibility of the total energy for AZO 500 nm and 900 nm for the nonlinear CPA.

4. Conclusions

We theoretically and experimentally demonstrate coherent control of absorption in films of ENZ material. We show that it is possible to achieve a coherent absorption-mediated interferometric effect with a maximum of its effect locked just below the λ_{ENZ} wavelength. Due the strong dispersion at wavelengths below the crossing point, it can be tuned to any wavelength shorter than λ_{ENZ} by varying film thickness and the optical losses. The 60% total visibility achieved in the AZO film could be improved using a CW and collimated beam in order to achieve CPA. By using AZO's strong intensity-dependent nonlinearities, we also showed that it is possible to dynamically tune the visibility of the total energy by simply increasing the intensity of the incoming beam. The possibility to add a degree of freedom for the coherent control of the absorption in ENZ media by using intensity-dependent refractive index proposes a route towards technologies [45] such as optical data processing or devices that require efficient light absorption and dynamical tunability. All the data supporting this manuscript are available at http://researchdata.gla.ac.uk/939/.

Author Contributions: Investigation and data curation V.B. and S.V.; Sample fabrication C.D.; code for analysis S.V. and V.B., and code for measurement acquisition T.R.; Formal analysis and writing-original draft V.B., S.V. and D.F.; supervision D.F., V.M.S., A.B. and M.F.; all the author have contributed equally to the writing—review. All authors have read and agreed to the published version of the manuscript.

Funding: D. F. acknowledges financial support from EPSRC (UK, Grant No. EP/M009122/1). The Purdue team acknowledges support by the U.S. Office of Naval Research (optical characterization), U.S. Department of Energy, Office of Basic Energy Sciences, Division of Materials Sciences and Engineering under Award DE-SC0017717 (sample preparation), and Air Force Office of Scientific Research (AFOSR) award FA9550-18-1-0002.

Conflicts of Interest: The authors declare no conflict of interest.

References

1. Chong, Y.; Ge, L.; Cao, H.; Stone, A.D. Coherent perfect absorbers: Time-reversed lasers. *Phys. Rev. Lett.* **2010**, *105*, 053901. [CrossRef] [PubMed]
2. Wan, W.; Chong, Y.; Ge, L.; Noh, H.; Stone, A.D.; Cao, H. Time-reversed lasing and interferometric control of absorption. *Science* **2011**, *331*, 889–892. [CrossRef] [PubMed]
3. Baranov, D.G.; Krasnok, A.; Shegai, T.; Alù, A.; Chong, Y. Coherent perfect absorbers: Linear control of light-with-light. *Nat. Rev. Mater.* **2017**, *2*, 17064. [CrossRef]
4. Zhang, J.; MacDonald, K.F.; Zheludev, N.I. Controlling light-with-light without nonlinearity. *Light Sci. Appl.* **2012**, *1*, e18. [CrossRef]
5. Kats, M.A.; Blanchard, R.; Genevet, P.; Capasso, F. Nanometre optical coatings based on strong interference effects in highly absorbing media. *Nat. Mater.* **2013**, *12*, 20. [CrossRef] [PubMed]
6. Rao, S.M.; Heitz, J.J.; Roger, T.; Westerberg, N.; Faccio, D. Coherent control of light interaction with graphene. *Opt. Lett.* **2014**, *39*, 5345–5347. [CrossRef]
7. Fang, X.; Lun Tseng, M.; Ou, J.Y.; MacDonald, K.F.; Ping Tsai, D.; Zheludev, N.I. Ultrafast all-optical switching via coherent modulation of metamaterial absorption. *Appl. Phys. Lett.* **2014**, *104*, 141102. [CrossRef]
8. Roger, T.; Restuccia, S.; Lyons, A.; Giovannini, D.; Romero, J.; Jeffers, J.; Padgett, M.; Faccio, D. Coherent absorption of N00N states. *Phys. Rev. Lett.* **2016**, *117*, 023601. [CrossRef]
9. Altuzarra, C.; Vezzoli, S.; Valente, J.; Gao, W.; Soci, C.; Faccio, D.; Couteau, C. Coherent perfect absorption in metamaterials with entangled photons. *ACS Photon.* **2017**, *4*, 2124–2128. [CrossRef]
10. Roger, T.; Vezzoli, S.; Bolduc, E.; Valente, J.; Heitz, J.J.; Jeffers, J.; Soci, C.; Leach, J.; Couteau, C.; Zheludev, N.I.; et al. Coherent perfect absorption in deeply subwavelength films in the single-photon regime. *Nat. Commun.* **2015**, *6*, 7031. [CrossRef]
11. Lyons, A.; Oren, D.; Roger, T.; Savinov, V.; Valente, J.; Vezzoli, S.; Zheludev, N.I.; Segev, M.; Faccio, D. Coherent metamaterial absorption of two-photon states with 40% efficiency. *Phys. Rev. A* **2019**, *99*, 011801. [CrossRef]
12. Wei, P.; Croënne, C.; Tak Chu, S.; Li, J. Symmetrical and anti-symmetrical coherent perfect absorption for acoustic waves. *Appl. Phys. Lett.* **2014**, *104*, 121902. [CrossRef]
13. Akhlaghi, M.K.; Schelew, E.; Young, J.F. Waveguide integrated superconducting single-photon detectors implemented as near-perfect absorbers of coherent radiation. *Nat. Commun.* **2015**, *6*, 8233. [CrossRef] [PubMed]
14. Bruck, R.; Muskens, O.L. Plasmonic nanoantennas as integrated coherent perfect absorbers on SOI waveguides for modulators and all-optical switches. *Opt. Express* **2013**, *21*, 27652–27661. [CrossRef]
15. Xomalis, A.; Demirtzioglou, I.; Plum, E.; Jung, Y.; Nalla, V.; Lacava, C.; MacDonald, K.F.; Petropoulos, P.; Richardson, D.J.; Zheludev, N.I. Fibre-optic metadevice for all-optical signal modulation based on coherent absorption. *Nat. Commun.* **2018**, *9*, 182. [CrossRef]
16. Papaioannou, M.; Plum, E.; Valente, J.; Rogers, E.T.; Zheludev, N.I. All-optical multichannel logic based on coherent perfect absorption in a plasmonic metamaterial. *APL Photon.* **2016**, *1*, 090801. [CrossRef]
17. Dutta-Gupta, S.; Martin, O.J.; Gupta, S.D.; Agarwal, G. Controllable coherent perfect absorption in a composite film. *Opt. Express* **2012**, *20*, 1330–1336. [CrossRef]
18. Villinger, M.L.; Bayat, M.; Pye, L.N.; Abouraddy, A.F. Analytical model for coherent perfect absorption in one-dimensional photonic structures. *Opt. Lett.* **2015**, *40*, 5550–5553. [CrossRef]
19. Zhao, B.; Zhao, J.; Zhang, Z. Enhancement of near-infrared absorption in graphene with metal gratings. *Appl. Phys. Lett.* **2014**, *105*, 031905. [CrossRef]

20. Kim, T.Y.; Badsha, M.A.; Yoon, J.; Lee, S.Y.; Jun, Y.C.; Hwangbo, C.K. General strategy for broadband coherent perfect absorption and multi-wavelength all-optical switching based on epsilon-near-zero multilayer films. *Sci. Rep.* **2016**, *6*, 22941. [CrossRef]
21. Naik, G.V.; Liu, J.; Kildishev, A.V.; Shalaev, V.M.; Boltasseva, A. Demonstration of Al: ZnO as a plasmonic component for near-infrared metamaterials. *Proc. Natl. Acad. Sci. USA* **2012**, *109*, 8834–8838. [CrossRef] [PubMed]
22. Naik, G.V.; Kim, J.; Boltasseva, A. Oxides and nitrides as alternative plasmonic materials in the optical range. *Opt. Mater. Express* **2011**, *1*, 1090–1099. [CrossRef]
23. Yoon, J.; Zhou, M.; Badsha, M.A.; Kim, T.Y.; Jun, Y.C.; Hwangbo, C.K. Broadband epsilon-near-zero perfect absorption in the near-infrared. *Sci. Rep.* **2015**, *5*, 12788. [CrossRef] [PubMed]
24. Badsha, M.A.; Jun, Y.C.; Hwangbo, C.K. Admittance matching analysis of perfect absorption in unpatterned thin films. *Opt. Commun.* **2014**, *332*, 206–213. [CrossRef]
25. Jin, Y.; Xiao, S.; Mortensen, N.A.; He, S. Arbitrarily thin metamaterial structure for perfect absorption and giant magnification. *Opt. Express* **2011**, *19*, 11114–11119. [CrossRef]
26. Feng, S.; Halterman, K. Coherent perfect absorption in epsilon-near-zero metamaterials. *Phys. Rev. B* **2012**, *86*, 165103. [CrossRef]
27. Luk, T.S.; Campione, S.; Kim, I.; Feng, S.; Jun, Y.C.; Liu, S.; Wright, J.B.; Brener, I.; Catrysse, P.B.; Fan, S.; et al. Directional perfect absorption using deep subwavelength low-permittivity films. *Phys. Rev. B* **2014**, *90*, 085411. [CrossRef]
28. Park, J.; Kang, J.H.; Liu, X.; Brongersma, M.L. Electrically tunable epsilon-near-zero (ENZ) metafilm absorbers. *Sci. Rep.* **2015**, *5*, 15754. [CrossRef]
29. Vincenti, M. Non-collinear counter-propagating beams in epsilon-near-zero films: Enhancement and inhibition of nonlinear optical processes. *J. Opt.* **2017**, *19*, 124015. [CrossRef]
30. Carnemolla, E.G.; Caspani, L.; DeVault, C.; Clerici, M.; Vezzoli, S.; Bruno, V.; Shalaev, V.M.; Faccio, D.; Boltasseva, A.; Ferrera, M. Degenerate optical nonlinear enhancement in epsilon-near-zero transparent conducting oxides. *Opt. Mater. Express* **2018**, *8*, 3392–3400. [CrossRef]
31. Clerici, M.; Kinsey, N.; DeVault, C.; Kim, J.; Carnemolla, E.G.; Caspani, L.; Shaltout, A.; Faccio, D.; Shalaev, V.; Boltasseva, A.; et al. Controlling hybrid nonlinearities in transparent conducting oxides via two-colour excitation. *Nat. Commun.* **2017**, *8*, 15829. [CrossRef] [PubMed]
32. Caspani, L.; Kaipurath, R.; Clerici, M.; Ferrera, M.; Roger, T.; Kim, J.; Kinsey, N.; Pietrzyk, M.; Di Falco, A.; Shalaev, V.M.; et al. Enhanced nonlinear refractive index in ϵ-near-zero materials. *Phys. Rev. Lett.* **2016**, *116*, 233901. [CrossRef] [PubMed]
33. Alam, M.Z.; De Leon, I.; Boyd, R.W. Large optical nonlinearity of indium tin oxide in its epsilon-near-zero region. *Science* **2016**, *352*, 795–797. [CrossRef] [PubMed]
34. Kim, J.; Carnemolla, E.G.; DeVault, C.; Shaltout, A.M.; Faccio, D.; Shalaev, V.M.; Kildishev, A.V.; Ferrera, M.; Boltasseva, A. Dynamic control of nanocavities with tunable metal oxides. *Nano Lett.* **2018**, *18*, 740–746. [CrossRef]
35. Reshef, O.; De Leon, I.; Alam, M.Z.; Boyd, R.W. Nonlinear optical effects in epsilon-near-zero media. *Nat. Rev. Mater.* **2019**, *4*, 535–551. [CrossRef]
36. Kinsey, N.; DeVault, C.; Boltasseva, A.; Shalaev, V.M. Near-zero-index materials for photonics. *Nat. Rev. Mater.* **2019**, *4*, 742–760. [CrossRef]
37. Vezzoli, S.; Bruno, V.; DeVault, C.; Roger, T.; Shalaev, V.M.; Boltasseva, A.; Ferrera, M.; Clerici, M.; Dubietis, A.; Faccio, D. Optical Time Reversal from Time-Dependent Epsilon-Near-Zero Media. *Phys. Rev. Lett.* **2018**, *120*, 043902, doi:10.1103/PhysRevLett.120.043902. [CrossRef]
38. Bruno, V.; DeVault, C.; Vezzoli, S.; Kudyshev, Z.; Huq, T.; Mignuzzi, S.; Jacassi, A.; Saha, S.; Shah, Y.D.; Maier, S.A.; et al. Negative refraction in time-varying, strongly-coupled plasmonic antenna-ENZ systems. *arXiv* **2019**, arXiv:1908.03908.
39. Campione, S.; Brener, I.; Marquier, F. Theory of epsilon-near-zero modes in ultrathin films. *Phys. Rev. B* **2015**, *91*, 121408. [CrossRef]
40. Cleary, J.W.; Smith, E.M.; Leedy, K.D.; Grzybowski, G.; Guo, J. Optical and electrical properties of ultra-thin indium tin oxide nanofilms on silicon for infrared photonics. *Opt. Mater. Express* **2018**, *8*, 1231–1245. [CrossRef]

41. Feigenbaum, E.; Diest, K.; Atwater, H.A. Unity-order index change in transparent conducting oxides at visible frequencies. *Nano Lett.* **2010**, *10*, 2111–2116. [CrossRef] [PubMed]
42. Kim, J.; Dutta, A.; Naik, G.V.; Giles, A.J.; Bezares, F.J.; Ellis, C.T.; Tischler, J.G.; Mahmoud, A.M.; Caglayan, H.; Glembocki, O.J.; et al. Role of epsilon-near-zero substrates in the optical response of plasmonic antennas. *Optica* **2016**, *3*, 339–346. [CrossRef]
43. DeVault, C.T.; Zenin, V.A.; Pors, A.; Chaudhuri, K.; Kim, J.; Boltasseva, A.; Shalaev, V.M.; Bozhevolnyi, S.I. Suppression of near-field coupling in plasmonic antennas on epsilon-near-zero substrates. *Optica* **2018**, *5*, 1557–1563. [CrossRef]
44. Khurgin, J.B.; Clerici, M.; Bruno, V.; Caspani, L.; DeVault, C.; Kim, J.; Shaltout, A.; Boltasseva, A.; Shalaev, V.M.; Ferrera, M.; et al. Adiabatic frequency conversion in epsilon near zero materials: It is all about group velocity. *arXiv* **2019**, arXiv:1906.04849.
45. Kinsey, N.; Ferrera, M.; Shalaev, V.; Boltasseva, A. Examining nanophotonics for integrated hybrid systems: A review of plasmonic interconnects and modulators using traditional and alternative materials. *JOSA B* **2015**, *32*, 121–142. [CrossRef]